Landé g Factor Measurement of $^{48}Ti^+$ Using Simultaneous Comagnetometry and Quantum Logic Spectroscopy

Till Rehmert,[1,2,*] Maximilian J. Zawierucha,[1,2] Sergey G. Porsev,[3] Kai Dietze,[1,2] Piet O. Schmidt,[1,2] Dmytro Filin,[3] Charles Cheung,[3] Marianna S. Safronova,[3] and Fabian Wolf[1,†]

[1]*Physikalisch-Technische Bundesanstalt, Bundesallee 100, 38116 Braunschweig, Germany*
[2]*Institut für Quantenoptik, Leibniz Universität Hannover, Welfengarten 1, 30167 Hannover, Germany*
[3]*Department of Physics and Astronomy, University of Delaware, Newark, Delaware 19716, USA*

(Received 21 August 2025; revised 14 November 2025; accepted 20 January 2026; published 27 February 2026)

We present a quantum logic scheme mitigating systematic effects in the measurement of magnetic properties of ions caused by temporal magnetic field fluctuations through comagnetometry. This is achieved through simultaneous interrogation of a spectroscopy ion and a cotrapped reference ion with a precisely known g factor confined in a Paul trap. This allows measurement of the ground state g factors of a single $^{48}Ti^+$ ion with uncertainties at the 10^{-6} level in the weak B-field regime. The experimental scheme can be applied to many ions, including those that cannot be directly laser cooled. We compare the experimentally determined g factors of $^{48}Ti^+$ with new theoretical predictions using a combination of configuration interaction and second-order many-body perturbation theory. Theory and experiment agree within the expected level of accuracy.

DOI: 10.1103/1x4h-5ycp

Landé g factors quantify magnetic moments associated with angular momenta of particles. Precise knowledge of these allows the use of atomic systems as magnetic field probes in laboratory [1–4] and astrophysical settings [5,6]. Currently, the most precise g factor measurements are performed in Penning traps [7]. There, g factors can be measured independent of the precise magnetic field strength by relating it to the trapping frequencies. This approach mitigates uncertainties due to magnetic field fluctuations, which would otherwise limit the achievable precision, allowing for determinations of g with an absolute uncertainty of $< 10^{-9}$ [8,9]. However, Penning traps operate at magnetic fields of several Tesla to confine the charged particle. Such high magnetic fields prevent the measurement of g_J factors for singly charged ions with weak LS-angular-momentum coupling, since orbital angular momentum (L) and electronic spin (S) are decoupled in the Paschen-Back regime. Furthermore, the extended averaging times required for these measurements in Penning traps hinder the accurate measurement of short-lived metastable states. Consequently, many atomic states lack precise g factor measurements and rely on theoretical calculations [10,11].

Here, we present a measurement scheme for accurate determinations of g factors in the weak B-field regime. This scheme is independent of the specific atomic species and based on quantum logic in a linear Paul trap. By simultaneously interrogating a cotrapped logic ion with a well-known g factor as a comagnetometer, our scheme enables precise measurements of the g factor for a wide variety of atomic states. Measurements of g factors relying on well-known reference states in the same species [12–14] and in cotrapped species [15–17], e.g., a cotrapped logic ion, are an established tool to reduce uncertainty due to insufficient knowledge and control over the magnetic field. Going beyond previous implementations for the weak B-field regime, we present a scheme, where the comagnetometer is not interrogated interleaved but simultaneously with the spectroscopy ion, resulting in suppression of systematic errors due to temporal magnetic field variations. Similar schemes have been demonstrated in Penning traps [18] as well as neutral atom experiments [17] and have been proposed for the characterization and mitigation of systematic errors in optical clocks [19,20]. We implement this scheme to determine the g factors of all four $|J\rangle$ states of the ground state a^4F of a single $^{48}Ti^+$ ion using the $^2S_{1/2}$ ground state in a $^{40}Ca^+$ ion as a comagnetometer.

Titanium is an element of significant astrophysical relevance, as its emission and absorption lines are present in many cosmic spectra, such as in stellar spectra [21] and quasar absorption spectra [22]. This provides valuable information for studies on the variation of fundamental constants [23] and stellar composition analysis [24]. The

*Contact author: till.rehmert@ptb.de
†Contact author: fabian.wolf@ptb.de

complex electronic structure of titanium arising from multiple valence electrons demands for advanced approaches in atomic structure calculations [25]. By comparing the experimentally obtained g factors to theoretical predictions, this Letter allows for the exploration of the role of negative energy states [26] and QED effects [27], thus advancing our understanding of fundamental physics in these systems.

The energy shift between adjacent angular momentum projection eigenstates $|m_J\rangle$ and $|m_J+1\rangle$ in a magnetic field B is given by

$$\Delta E = g\mu_{\mathrm{B}}B + g^{(2)}\frac{(\mu_{\mathrm{B}}B)^2}{m_e c^2} + \mathcal{O}(B^3) \tag{1}$$

with the Landé g factor, the Bohr magneton μ_{B}, the electron mass m_e, and the speed of light c. $g^{(2)}$ denotes the second-order Zeeman coefficient. Since the g factor for the $^2S_{1/2}$ state in $^{40}\mathrm{Ca}^+$ is precisely known from Penning trap experiments [28], measurement of the $^2S_{1/2}$ Zeeman splitting energy ΔE_{Ca} during the experimental sequence determines the magnetic field at the position of the ion. Assuming a spatially homogeneous magnetic field, the g factor of $^{48}\mathrm{Ti}^+$, labeled as g_{Ti}, can, to first order, be inferred from

$$g_{\mathrm{Ti}} = g_{\mathrm{Ca}}\frac{\Delta E_{\mathrm{Ti}}}{\Delta E_{\mathrm{Ca}}}, \tag{2}$$

where g_{Ca} is the g factor for the cotrapped calcium ground state [28], and ΔE_{Ti} and ΔE_{Ca} are the Zeeman energy splittings for titanium and calcium, respectively. In Eq. (2), higher-order contributions to ΔE can be neglected due to sufficiently small $g^{(2)}$ coefficients for the $^{40}\mathrm{Ca}^+$ $^2S_{1/2}$ and the $^{48}\mathrm{Ti}^+$ $\mathrm{a}^4\mathrm{F}$ fine structure states. A detailed discussion of the method of calculating $g^{(2)}$ and the resulting corrections to g_{Ti} are given in Supplemental Material [29].

Experimental setup—The measurement scheme is realized in a linear segmented Paul trap. A detailed discussion on the design of the trap can be found in Refs. [47,48]. A two-ion crystal composed of one $^{40}\mathrm{Ca}^+$ and one $^{48}\mathrm{Ti}^+$ ion is prepared by loading multiple ions of each species and splitting the resulting crystal until the desired configuration is obtained [48]. A detailed description of the implemented quantum logic methods is given in Ref. [30]; in the following, the most relevant aspects are summarized. Operations coupling the $|\downarrow\rangle = |S_{1/2}, m_J = -1/2\rangle$ and the $|\uparrow\rangle = |D_{5/2}, m_J = -1/2\rangle$ optical qubit states on the $^{40}\mathrm{Ca}^+$ logic ion are performed with a narrow-linewidth laser at 729 nm. A pair of magnetic field coils generates a magnetic field of 0.397 mT, which defines a quantization axis and results in a $^{40}\mathrm{Ca}^+$ ground state splitting of $\sim$11.135 MHz. An active stabilization compensates for magnetic field drifts using a feedback loop. $^{48}\mathrm{Ti}^+$ state

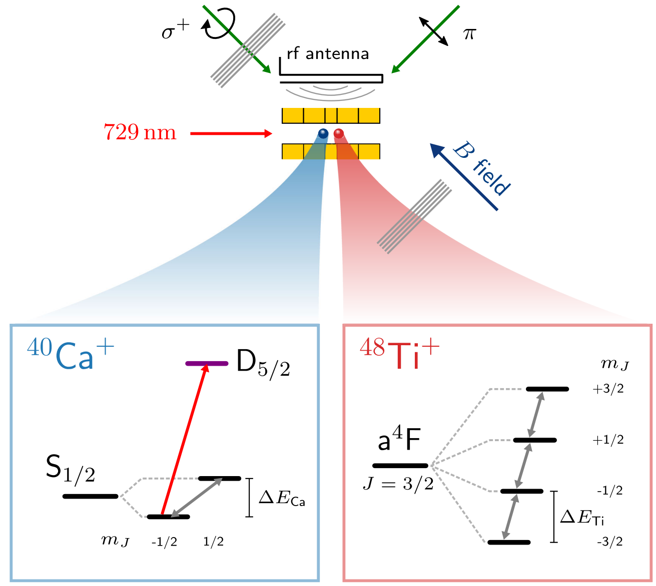

FIG. 1. Two-ion crystal trapped in a segmented Paul trap. A pair of magnetic field coils in Helmholtz-like configuration generates a magnetic field that defines a quantization axis (blue arrow) and lifts the degeneracy of the fine structure states in $^{40}\mathrm{Ca}^+$ and $^{48}\mathrm{Ti}^+$ into Zeeman states. An in-vacuum antenna couples states with frequency splittings in the kilo- to megahertz regime (gray arrows). State readout on the logic ion's qubit transition is realized using a highly stable laser at 729 nm (red arrow). Zeeman state preparation in $^{48}\mathrm{Ti}^+$ and quantum logic readout is facilitated using a far-detuned laser (green arrows) driving Raman transitions.

preparation and quantum logic readout is facilitated using a far-detuned laser [30,49] with a wavelength of 532 nm driving Raman transitions. Polarization and orientation of the two Raman beams with respect to the trap axis allow population transfer between adjacent Zeeman states as well as exciting motional modes of the two-ion ensemble. This way, state information from the spectroscopy ion can be transferred to the shared motional state and read out on the logic ion. Radio frequency (rf) fields from an in-vacuum antenna can couple Zeeman states on both the calcium and the titanium ion. Figure 1 depicts the logic ion and the spectroscopy ion confined in the trap, including the relevant levels for the measurement scheme. Arrows indicate the directions and polarizations of the relevant lasers for state manipulation, as well as the orientation of the magnetic field with respect to the trap.

Measurement of g factors—The experimental sequence for simultaneously probing Zeeman transitions in the spectroscopy and the logic ion starts with ground state cooling (GSC), realized by a combination of Doppler, electromagnetically-induced-transparency (EIT) cooling, and sideband cooling. The preparation of a stretched state ($|m_J = \pm J\rangle_{\mathrm{Ti}}$) in one of the four $\mathrm{a}^4\mathrm{F}_J$ ($J \in \{3/2, 5/2, 7/2, 9/2\}$) ground states of $^{48}\mathrm{Ti}^+$ is achieved by population transfer pulses on a common motional red sideband that are rendered irreversible

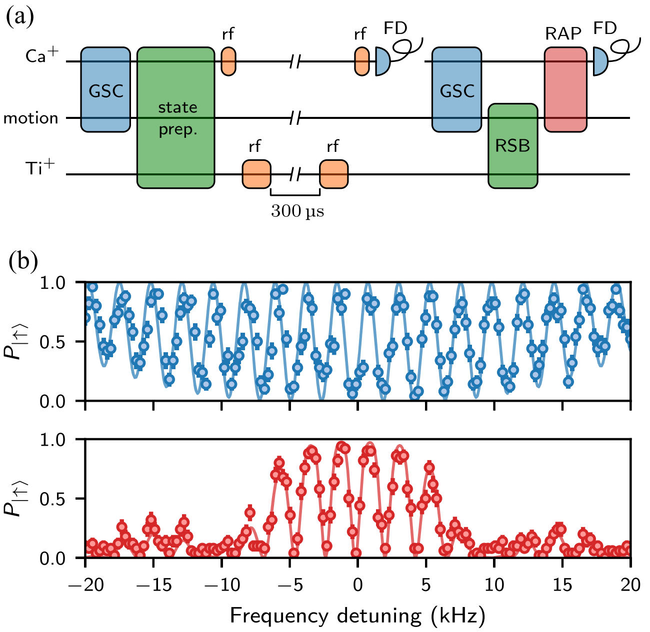

FIG. 2. Simultaneous rf Ramsey spectroscopy on $^{48}\mathrm{Ti}^+$ and $^{40}\mathrm{Ca}^+$. (a) Experimental sequence starting with motional ground state cooling followed by the preparation of a $|J, m_J = -J\rangle_{\mathrm{Ti}}$ stretched state in the a^{4}F electronic ground state. Two rf pulses open Ramsey interferometers on the calcium and titanium ion, sequentially. After a common wait time of 300 μs, two additional pulses close the interferometers. After state detection on the $^{40}\mathrm{Ca}^+$ qubit transition, the $^{48}\mathrm{Ti}^+$ Zeeman state distribution is mapped to $^{40}\mathrm{Ca}^+$ after additional GSC and by a red sideband (RSB) RAP pulse with the Raman laser on $^{48}\mathrm{Ti}^+$. (b) Ramsey fringes for the $^{40}\mathrm{Ca}^+$ ground state (upper) and titanium a^{4}F ($J = 3/2$) state (lower). Solid lines are fits to experimental data. Note the narrower downward peaks of the fringes for $^{48}\mathrm{Ti}^+$ resulting from a spin rotation in a system with four levels.

by GSC on $^{40}\mathrm{Ca}^+$ [30,50]. A Ramsey interferometer is opened on both the $^{40}\mathrm{Ca}^+$ $^2S_{1/2}$ state and one of the $^{48}\mathrm{Ti}^+$ a^{4}F states by applying two rf pulses with individual times of $t_\pi^{\mathrm{Ca}}/2$ ($t_\pi^{\mathrm{Ti}}/2$) with t_π being the time required for a rotation of the angular momentum by an angle $\theta = \pi$. After a Ramsey dark time of t_R^{Ca} (t_R^{Ti}), the two Ramsey interferometers are closed by a $t_\pi/2$ pulse on each species. This Ramsey interferometry sequence converts phase differences between the local rf oscillator and atomic transition frequency to detectable Zeeman population imbalances in $^{40}\mathrm{Ca}^+$ and $^{48}\mathrm{Ti}^+$ Zeeman manifolds. The $^{40}\mathrm{Ca}^+$ state is read out through fluorescence detection (FD) after shelving the Zeeman state information to state $|\uparrow\rangle$ of the optical qubit. The photon scattering during the detection introduces motion to the system but does not change the population distribution in the $^{48}\mathrm{Ti}^+$ Zeeman manifold. Next, the $^{48}\mathrm{Ti}^+$ Zeeman population is read out using quantum logic. This is accomplished by cooling to the motional ground state using the calcium logic ion and mapping the $^{48}\mathrm{Ti}^+$ Zeeman population to a motional mode of the two-ion crystal, which is finally read out at the $^{40}\mathrm{Ca}^+$ ion by a rapid-adiabatic-passage (RAP) pulse on a red sideband of the calcium qubit transition [51]. The full experimental sequence is visualized in Fig. 2(a). In Fig. 2(b), a typical measurement result using $t_R^{\mathrm{Ti}} = 300$ μs and $t_R^{\mathrm{Ca}} = t_R^{\mathrm{Ti}} + t_\pi^{\mathrm{Ti}}$ is shown. The Ramsey fringes for $^{48}\mathrm{Ti}^+$ are narrower compared to $^{40}\mathrm{Ca}^+$, since they result from a spin rotation in a system with more than two levels. A detailed description of the fit function used in Fig. 2(b) is provided in Supplemental Material [29].

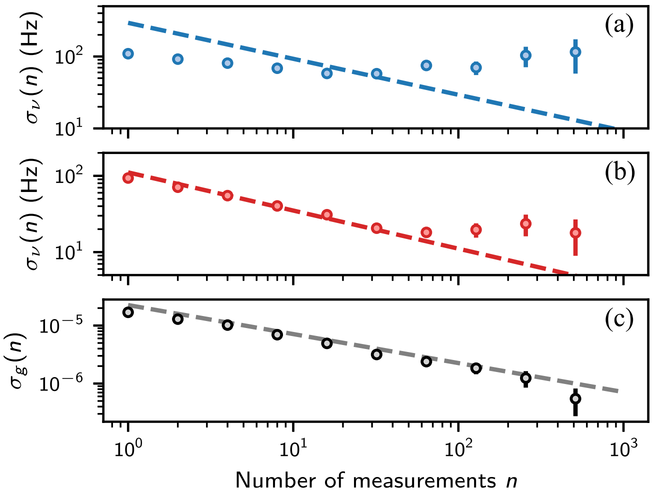

FIG. 3. Measurement of the g factor of state $|J = 3/2\rangle$ in the a^{4}F ground state. (a),(b) Allan deviation $\sigma_\nu(n)$ of the measured $^{40}\mathrm{Ca}^+$ $S_{1/2}$ ground state splitting (blue dots) and the $^{48}\mathrm{Ti}^+$ $|J = 3/2, m_J\rangle \to |J = 3/2, m_J - 1\rangle$ state splitting (red dots), respectively. (c) Allan deviation of the calculated g factor. Dashed lines indicate expected white noise scaling $\sigma_{\mathrm{std}}/\sqrt{n}$, where σ_{std} is the standard deviation of the collected data.

To follow magnetic field drifts, the applied frequency of the rf pulses was kept on resonance using two individual servo loops [52]. For each $^{48}\mathrm{Ti}^+$ ion fine structure state, at least 1000 lock iterations, each comprising ten measurement repetitions, were recorded. The Zeeman splitting frequency stabilities are analyzed using Allan deviations, depicted in Figs. 3(a) and 3(b) for the calcium and the titanium ion, respectively. An Allan deviation for quantum projection noise-limited measurements averages down with

TABLE I. Corrections and systematic uncertainties of the measured g factors. Corrections to the measured values, $\Delta g_{\mathrm{ac,trap}}$ and Δg_{grad}, arise from the oscillating trap magnetic field and the static magnetic field gradient, respectively. Systematic uncertainties of the corrections are given in brackets.

State	$\Delta g_{\mathrm{ac,trap}} \times 10^6$	$\Delta g_{\mathrm{grad}} \times 10^6$
a^{4}F$_{3/2}$	24(1)	< 1(1)
a^{4}F$_{5/2}$	51(2)	< 2(4)
a^{4}F$_{7/2}$	53(2)	< 2(4)
a^{4}F$_{9/2}$	52(2)	< 2(5)

TABLE II. Theoretical and experimental values of the $^{48}Ti^{+}$ g factors. g_{LS} denotes g factor values calculated taking only LS coupling into account. The experimental values include correction from the ac-Zeeman shift. Statistical uncertainties of the experimental values were derived from Allan deviations of the calculated data for the g factors. Errors given in experiment column are the statistical and total systematic uncertainties.

State	g_{LS}	Theory [10,11]	Theory (this Letter)	Experiment (this Letter)
$a^4F_{3/2}$	0.39990	0.39853	0.3986	$0.3984860(5)_{\mathrm{stat}}(1)_{\mathrm{sys}}$
$a^4F_{5/2}$	1.02858	1.02840	1.0284	$1.028369(2)_{\mathrm{stat}}(4)_{\mathrm{sys}}$
$a^4F_{7/2}$	1.23813	1.23839	1.2384	$1.238378(2)_{\mathrm{stat}}(4)_{\mathrm{sys}}$
$a^4F_{9/2}$	1.33339	1.33388	1.3339	$1.333875(4)_{\mathrm{stat}}(5)_{\mathrm{sys}}$

$\propto \sqrt{1/n}$ corresponding to white frequency noise, where n is the number of measurements. For $^{48}Ti^{+}$ white noise behavior is observed only on short timescales. On longer timescales, the frequency variation is dominated by magnetic field fluctuations resulting in a deviation from the $\sqrt{1/n}$ scaling of the Allan deviation. Because of its higher g factor, $^{40}Ca^{+}$ is more sensitive to fluctuations in the magnetic field. As a result, field variations already dominate the Allan deviation on timescales where the servo can track the line accounting for the deviation of all the $^{40}Ca^{+}$ points from the $\sqrt{1/n}$ scaling in Fig. 3(a). However, the recovery of the white frequency noise scaling of the Allan deviation for g_{Ti} demonstrates the robustness of the scheme against such fluctuations [see Fig. 3(c)]. This enables a determination of the g factor with a statistical uncertainty on the 10^{-6} level. The final statistical uncertainties are limited by the measurement time (for details see Supplemental Material [29]). Systematic effects, such as the electric quadrupole shift and the nonlinear Zeeman effect are estimated to be well below the statistical uncertainties. However, trap-drive-induced ac-Zeeman shifts result in a significant shift, $\Delta g_{\mathrm{ac,trap}}$, of the measured g factors. The final systematic accuracy of the measured g factors is limited by the uncertainty of the static magnetic field gradient, $\sigma_{\Delta g_{\mathrm{grad}}}$, resulting in different magnetic field strengths for the two ion positions and the uncertainty in the determination of the oscillating trap magnetic field that causes the ac-Zeeman shift. The former uncertainty is assumed to partially average out due to switches in the ions' positions and could be further reduced by controlling the ordering of the two-ion crystal or by installing gradient compensation coils. Leading corrections and their uncertainties are summarized in Table I. A detailed discussion of all systematic shifts can be found in Supplemental Material [29]. The measured g factors for the fine structure of the a^4F ground states including corrections from ac-Zeeman shifts are summarized in Table II.

A large fraction of the magnetic field noise in this experiment originates from the ac line and is therefore most prevalent at multiples of 50 Hz. Its influence was analyzed by measuring the g factor of the $|J=3/2\rangle_{\mathrm{Ti}}$ state for different time delays between the start of the experimental sequence and the ac line [53]. As shown in Fig. 4, both frequency measurements vary according to the changing magnetic field, while the variation of the extracted g factor is strongly suppressed. This demonstrates the success of the comagnetometry Ramsey scheme.

Theory—In addition to the experimental determination of the a^4F g factors, we have performed theoretical calculations using an approach combining the configuration interaction (CI) with the second-order many-body perturbation (MBPT) method [34,35] (see Supplemental Material [29] for more information). A pure CI calculation, together with the multiconfigurational Dirac-Fock approach used in Ref. [10], accounts for valence-valence correlations, whereas MBPT describes core-valence correlations. When combined within the CI + MBPT framework, these methods enable a simultaneous treatment of both types of correlations. Our analysis demonstrates a low

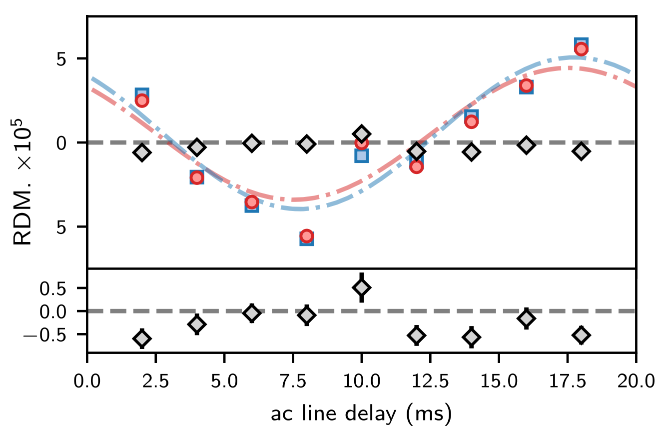

FIG. 4. Measurement of the $|J=3/2\rangle_{\mathrm{Ti}}$ state's g factor in dependence of an additional delay between the ac line trigger and the start of the experimental sequence. Blue squares, relative deviation from the mean (RDM) of all frequency data of the measured $^{40}Ca^{+}$ $S_{1/2}$ splitting; red circles, relative deviation from the mean of all frequency data of the measured Zeeman splitting in the $^{48}Ti^{+}$ $J=3/2$ manifold. For the frequency data, error bars indicate standard error of the mean. Black diamonds, extracted g factor; errors indicate statistical uncertainty propagated from the uncertainty of the frequency measurements. Sine functions were fitted to the frequency data to guide the eye. Lower: deviation of the extracted g factor from the mean value (dashed line).

sensitivity of the g factors presented in Table II to the core-valence correlations. The g factors obtained within the framework of CI + MBPT are only slightly [by $\sim(3\text{–}5) \times 10^{-5}$] larger than the pure CI values. Our Letter demonstrated that these core-valence correlations already contribute at that level of accuracy. This implies that the additional digits reported in Ref. [10] were not intended to be taken as significant, as no theoretical uncertainty was provided.

Our results show only a small discrepancy with the experimental data. The small residual difference between theory and experiment cannot be analyzed within the accuracy of the present calculations. Higher-order QED contributions and the effects of negative-energy states, which are not included in our approach, may contribute at the level of the achieved experimental precision [29]. In few-electron systems, such as highly charged ions, it has been shown that the inclusion of these contributions lead to a better agreement of the theory with the experimental data [16]. The theoretical and experimental values for the g factors from this Letter as well as the theoretical values from Refs. [10,11] are listed in Table II.

Conclusion—We have measured the Landé g factors of a single ion with an absolute uncertainty on the 10^{-6} level by using a simultaneous Ramsey interrogation on a Zeeman transition of a cotrapped logic ion in a Paul trap. The low uncertainty is enabled by a strong suppression of magnetic field noise-induced systematic errors using this comagnetometry scheme. The presented method is transferable to other trapped ion systems and allows one to put strong bounds on QED and negative-energy state contributions for systems where theory and experiment achieve similar accuracy. In addition, the precise knowledge of magnetic properties in atomic species is relevant for the determination of systematic effects in many applications such as optical atomic clocks or in high-precision spectroscopy in general. Further, we provide new theoretical values for the g factors and see a good agreement with other theoretical predictions [10]. This measurement constitutes the first g factor measurement of the $^{48}Ti^{+}$ ground state.

Acknowledgments—We thank Martin Steinel for helpful comments on the manuscript and Jonathan Morgner for discussions on Penning trap g factor measurements. Furthermore, we thank the aluminium optical clock team for providing stable light at 729 nm. This research was funded by the Deutsche Forschungsgemeinschaft (DFG, German Research Foundation)—Project-No. 274200144—SFB 1227 (DQ-mat) B05 with partial support from Germany's Excellence Strategy EXC-2123 QuantumFrontiers No. 390837967. The project has received funding from the European Research Council (ERC) under the European Union's Horizon 2020 research and innovation program (Grant Agreement No. 101019987). The calculations in this work were done through the use of Information Technologies resources at the University of Delaware, specifically the high-performance Caviness and DARWIN computer clusters. The theoretical work has been supported in part by the U.S. NSF Grants No. PHY-2309254 and No. OAC-2209639, U.S. Office of Naval Research Grant No. N000142512105, and by the European Research Council (ERC) under the Horizon 2020 Research and Innovation Program of the European Union (Grant Agreement No. 856415).

Data availability—The data that support the findings of this article are not publicly available upon publication because it is not technically feasible and/or the cost of preparing, depositing, and hosting the data would be prohibitive within the terms of this research project. The data are available from the authors upon reasonable request.

[1] M. Farooq, T. Chupp, J. Grange, A. Tewsley-Booth, D. Flay, D. Kawall, N. Sachdeva, and P. Winter, Phys. Rev. Lett. **124**, 223001 (2020).

[2] J. Shen, A. Borodin, and S. Schiller, Eur. Phys. J. D **68**, 359 (2014).

[3] I. Baumgart, J.-M. Cai, A. Retzker, M. B. Plenio, and C. Wunderlich, Phys. Rev. Lett. **116**, 240801 (2016).

[4] T. Ruster, H. Kaufmann, M. A. Luda, V. Kaushal, C. T. Schmiegelow, F. Schmidt-Kaler, and U. G. Poschinger, Phys. Rev. X **7**, 031050 (2017).

[5] P. Judge, Can. J. Phys. **95**, 847 (2017).

[6] A. Kawka and S. Vennes, Astron. Astrophys. **532**, A7 (2011).

[7] G. Werth, S. Sturm, and K. Blaum, in *Advances In Atomic, Molecular, and Optical Physics* (Elsevier, New York, 2018), Vol. 67, pp. 257–296.

[8] L. S. Brown and G. Gabrielse, Phys. Rev. A **25**, 2423 (1982).

[9] S. Sturm, G. Werth, and K. Blaum, Ann. Phys. (Berlin) **525**, 620 (2013).

[10] W. Li, P. Rynkun, L. Radžiūtė, G. Gaigalas, B. Atalay, A. Papoulia, K. Wang, H. Hartman, J. Ekman, T. Brage, C. Y. Chen, and P. Jönsson, Astron. Astrophys. **639**, A25 (2020).

[11] W. Li, P. Rynkun, L. Radziute, G. Gaigalas, B. Atalay, A. Papoulia, K. Wang, H. Hartman, J. Ekman, T. Brage, C. Y. Chen, and P. Jonsson, 10.26093/CDS/VIZIER.36390025 (2020).

[12] M. R. Hoffman, T. W. Noel, C. Auchter, A. Jayakumar, S. R. Williams, B. B. Blinov, and E. N. Fortson, Phys. Rev. A **88**, 025401 (2013).

[13] P. Micke, T. Leopold, S. A. King, E. Benkler, L. J. Spieß, L. Schmöger, M. Schwarz, J. R. C. López-Urrutia, and P. O. Schmidt, Nature (London) **578**, 60 (2020).

[14] Z. Ma, B. Zhang, Y. Huang, R. Hu, M. Zeng, K. Gao, and H. Guan, Phys. Rev. A **110**, 063102 (2024).

[15] T. Rosenband, P. O. Schmidt, D. B. Hume, W. M. Itano, T. M. Fortier, J. E. Stalnaker, K. Kim, S. A. Diddams, J. C. J. Koelemeij, J. C. Bergquist, and D. J. Wineland, Phys. Rev. Lett. **98**, 220801 (2007).

[16] L. J. Spieß, S. Chen, A. Wilzewski, M. Wehrheim, J. Gilles, A. Surzhykov, E. Benkler, M. Filzinger, M. Steinel, N. Huntemann, C. Cheung, S. G. Porsev, A. I. Bondarev,

M. S. Safronova, J. R. Crespo López-Urrutia, and P. O. Schmidt, Phys. Rev. Lett. **135**, 043002 (2025).
[17] P. Thekkeppatt, Digvijay, A. Urech, F. Schreck, and K. van Druten, Phys. Rev. Lett. **135**, 193001 (2025).
[18] T. Sailer, V. Debierre, Z. Harman, F. Heiße, C. König, J. Morgner, B. Tu, A. V. Volotka, C. H. Keitel, K. Blaum, and S. Sturm, Nature (London) **606**, 479 (2022).
[19] N. Akerman and R. Ozeri, New J. Phys. **20**, 123026 (2018).
[20] F. Wolf, Phys. Rev. Lett. **132**, 083202 (2024).
[21] N. C. Deb, A. Hibbert, Z. Felfli, and A. Z. Msezane, J. Phys. B **42**, 015701 (2009).
[22] C. Péroux, V. P. Kulkarni, J. Meiring, R. Ferlet, P. Khare, J. T. Lauroesch, G. Vladilo, and D. G. York, Astron. Astrophys. **450**, 53 (2006).
[23] M. T. Murphy and J. C. Berengut, Mon. Not. R. Astron. Soc. **438**, 388 (2013).
[24] P. Scott, M. Asplund, N. Grevesse, M. Bergemann, and A. Jacques Sauval, Astron. Astrophys. **573**, A26 (2015).
[25] M. S. Safronova, M. G. Kozlov, W. R. Johnson, and D. Jiang, Phys. Rev. A **80**, 012516 (2009).
[26] E. Lindroth and A. Ynnerman, Phys. Rev. A **47**, 961 (1993).
[27] D. E. Maison, L. V. Skripnikov, and D. A. Glazov, Phys. Rev. A **99**, 042506 (2019).
[28] G. Tommaseo, T. Pfeil, G. Revalde, G. Werth, P. Indelicato, and J. P. Desclaux, Eur. Phys. J. D **25**, 113 (2003).
[29] See Supplemental Material at http://link.aps.org/supplemental/10.1103/1x4h-5ycp for details on Ramsey spectroscopy in a qudit system, which also includes Refs. [30–33], details on the theoretical calculation of the g factors, which also includes Refs. [25,34–38], for statistical error determination, and for systematic error determination, which also includes Refs. [28,30,39–46].
[30] T. Rehmert, M. J. Zawierucha, K. Dietze, P. O. Schmidt, and F. Wolf, Phys. Rev. Lett. **134**, 113201 (2025).
[31] N. F. Ramsey, Phys. Rev. **78**, 695 (1950).
[32] F. T. Hioe, J. Opt. Soc. Am. B **4**, 1327 (1987).
[33] M. M. Hamermesh, *Group Theory and its Application to Physical Problems*, Addison-Wesley Series in Physics (Addison-Wesley Pub. Co Reading, Massachusetts, 1962).
[34] V. A. Dzuba, V. V. Flambaum, and M. G. Kozlov, Phys. Rev. A **54**, 3948 (1996).
[35] C. Cheung, M. G. Kozlov, S. G. Porsev, M. S. Safronova, I. I. Tupitsyn, and A. I. Bondarev, Comput. Phys. Commun. **308**, 109463 (2025).
[36] M. G. Kozlov, S. G. Porsev, and V. V. Flambaum, J. Phys. B **29**, 689 (1996).
[37] M. G. Kozlov, S. G. Porsev, M. S. Safronova, and I. I. Tupitsyn, Comput. Phys. Commun. **195**, 199 (2015).
[38] Yu. Ralchenko, A. Kramida, and J. Reader (The NIST ASD Team), NIST Atomic Spectra Database (version 4.1), (National Institute of Standards and Technology, Gaithersburg, MD, 2011), Available at http://physics.nist.gov/asd.
[39] H. C. J. Gan, G. Maslennikov, K.-W. Tseng, T. R. Tan, R. Kaewuam, K. J. Arnold, D. Matsukevich, and M. D. Barrett, Phys. Rev. A **98**, 032514 (2018).
[40] S. H. Autler and C. H. Townes, Phys. Rev. **100**, 703 (1955).
[41] W. M. Itano, J. Res. NIST **105**, 829 (2000).
[42] R. Shaniv, N. Akerman, and R. Ozeri, Phys. Rev. Lett. **116**, 140801 (2016).
[43] J. R. P. Angel, P. G. H. Sandars, and G. K. Woodgate, J. Chem. Phys. **47**, 1552 (1967).
[44] C. F. Roos, arXiv:quant-ph/0508148.
[45] D. A. Varshalovich, A. N. Moskalev, and V. K. Khersonskii, *Quantum Theory of Angular Momentum* (World Scientific, Singapore, 1988).
[46] S. G. Porsev, M. G. Kozlov, and M. S. Safronova, Phys. Rev. A **108**, L051102 (2023).
[47] T. Leopold, S. A. King, P. Micke, A. Bautista-Salvador, J. C. Heip, C. Ospelkaus, J. R. Crespo López-Urrutia, and P. O. Schmidt, Rev. Sci. Instrum. **90**, 073201 (2019).
[48] M. J. Zawierucha, T. Rehmert, J. Keller, T. E. Mehlstäubler, P. O. Schmidt, and F. Wolf, Phys. Rev. A **110**, 013107 (2024).
[49] C.-w. Chou, C. Kurz, D. B. Hume, P. N. Plessow, D. R. Leibrandt, and D. Leibfried, Nature (London) **545**, 203 (2017).
[50] P. O. Schmidt, T. Rosenband, C. Langer, W. M. Itano, J. C. Bergquist, and D. J. Wineland, Science **309**, 749 (2005).
[51] F. Gebert, Y. Wan, F. Wolf, J. C. Heip, and P. O. Schmidt, New J. Phys. **18**, 013037 (2016).
[52] E. Peik, T. Schneider, and C. Tamm, J. Phys. B **39**, 145 (2006).
[53] F. Schmidt-Kaler, S. Gulde, M. Riebe, T. Deuschle, A. Kreuter, G. Lancaster, C. Becher, J. Eschner, H. Häffner, and R. Blatt, J. Phys. B **36**, 623 (2003).